River Flow 2002, Bousmar & Zech (eds.)

Analysis on the flood flow storage in compound meandering channels by using unsteady two dimensional numerical model

A. Watanabe & S. Fukuoka
Graduate School of Engineering, Hiroshima University, Higashi-Hiroshima City, Japan

A.G. Mutasingwa
Student of Doctor Course, Graduate School of Engineering, Hiroshima University, Higashi-Hiroshima City, Japan

ABSTRACT: In a compound meandering channel, flood hydrograph deformation and attenuation of peak discharge occur as flood propagates downstream. It is important to make clear about the distortion of hydrograph and the reduction of peak discharge for river improvement planning. In this paper, this distortion process of hydrograph is simulated by using the unsteady 2D numerical model applied to the measured hydraulic data of flood flow in physical model experiments and Maruyama River, Japan.

1 INTRODUCTION

Longitudinal distributions of maximum water level and velocity of the design flood are necessary for river planning and design. These are generally calculated by the steady non-uniform flow analysis for a given maximum flood. In this analysis, the steady state is assumed and the roughness is evaluated inversely from observed data.

However, various hydraulic phenomena occur due to the unsteadiness of flood, as flow conditions are unsteady during the flood. The peak discharge is attenuated in the downstream direction because of water storage over the flood plain (Fukuoka et al. 2000a, b, c, 2001) and the additional resistance due to the momentum exchange between main channel and flood plains in a compound meandering channel (Fukuoka et al. 1998, 1999).

Even if the water levels at the rising and falling stage are same, the discharge is different. The discharge at rising stage is larger than that at falling stage, as the water surface slope at the rising stage is larger. When the water level rises over the flood plain height, the temporal changing rate in discharge decreases due to flow entering into flood plain and it increases due to flow entering from flood plain when the water level drops under the flood plain height. Because of this reason, the discharge hydrograph is distorted in the downstream direction and the peak discharge decreases with the movement of the flood wave.

In steady flow analysis, the effects of unsteadiness are considered virtually in the form of change of the channel roughness coefficient and the attenuation of the peak discharge is not considered in river planning. Therefore, we have to estimate the longitudinal change in the peak discharge for proper river planning. However, the evaluation of the peak discharge attenuation is difficult, because this hydraulic phenomenon is closely related to plan shape, cross sectional shape, roughness of the river, the unsteadiness of flood and so on.

This paper proposes an unsteady two dimensional numerical model which evaluates the change in hydrograph and attenuation of the peak discharge of flood flow for physical model experiments and the Maruyama River.

It has been known that a compound meandering channel flow has a three dimensional structure when the relative depth is large. At large relative depth, a 2D two-layered model is required at least for the computation of momentum exchange between the main channel and flood plain. However, the relative depth of most rivers is not so large for a flood event. In addition, the cost and time of computation are high for the long reach of rivers. Therefore, an unsteady two dimensional model expressed in terms of physical components in the general curvilinear coordinate system was chosen here, instead of using three dimensional model or 2D two-layered model.

2 METHOD OF ANALYSIS

2.1 *Introduction of general curvilinear coordinates system expressed by physical components*

In the fluid analysis, the general curvilinear coordinate system is often used to be able to introduce easily the complex boundary shape into the numerical model. However, in general cases, the physical meaning of each term in transformed form of basic equations is hard to understand and boundary conditions for shear stress terms are not clear yet. If the upwind scheme is used for the convection terms expressed by some general metrics tensors, the numerical solution depends on the grid layout and coordinate system because of the upwind on the metrics. In addition, when both velocity-vectors in general contra-variant components and original orthogonal components exist in a basic equation, the analysis may become complicated due to boundary shapes and arrangements of variables and grid points.

On the other hand, the orthogonal curvilinear coordinates system is often used for the analysis on the river flow. In this case, the physical meaning of each term in a basic equation is clear. But, when a coordinate system given for numerical computation is not precisely orthogonal, the accuracy of computation result is compromised.

In this paper, the equation of motion and continuity equation expressed by only physical contra-variant vectors in a physical curvilinear coordinates system are used to avoid all problems mentioned above. The normal differential method is used in a computation scheme.

2.2 *Basic equations*

The basic equations for unsteady 2D shallow water flow are transformed to those expressed by using physical contra-variant vectors, angles between each contra-variant axis, and physical contra-variant length in the physical curvilinear system as shown in Figure 1. The contra-variant base vector whose physical length is unity is defined by equation (1).

$$\begin{pmatrix} \tilde{\xi}_x & \tilde{\xi}_y \\ \tilde{\eta}_x & \tilde{\eta}_y \end{pmatrix} = \begin{pmatrix} d\xi \cdot \xi_x & d\xi \cdot \xi_y \\ d\eta \cdot \eta_x & d\eta \cdot \eta_y \end{pmatrix} \tag{1}$$

$$d\xi^2 = 1/(\xi_x^2 + \xi_y^2) \qquad d\eta^2 = 1/(\eta_x^2 + \eta_y^2)$$

where (x, y) is an arbitrary orthogonal coordinate system. Subscripts mean the partial derivatives with respect to (x, y) and $\sim$ physical components. Area of computational cell J and angles between contra-variant axis; $\theta^{\eta\xi}$ are defined by

$$J = x_\xi y_\eta - x_\eta y_\xi = 1/(\xi_x \eta_y - \xi_y \eta_x)$$

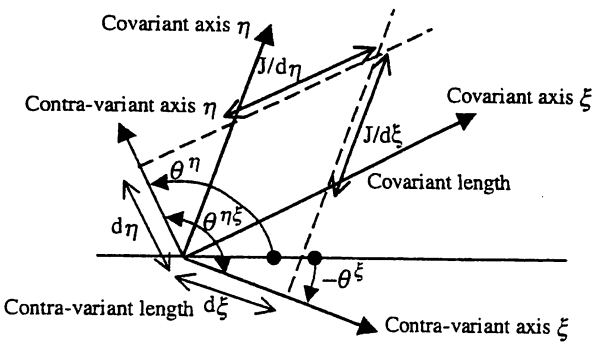

Figure 1. Definition of coordinate system and contra-variant length of computational mesh.

$$\tilde{J} = \frac{J}{d\xi \cdot d\eta} = \frac{1}{\sin\theta^{\eta\xi}}$$

$$\cos\theta^{\eta\xi} = (\tilde{\xi}_x, \tilde{\xi}_y)^T \cdot (\tilde{\eta}_x, \tilde{\eta}_y)$$

The relationship between velocity vectors in the orthogonal coordinate system and the physical general coordinate system is expressed as

$$\begin{pmatrix} \tilde{U} \\ \tilde{V} \end{pmatrix} = \begin{pmatrix} \tilde{\xi}_x & \tilde{\xi}_y \\ \tilde{\eta}_x & \tilde{\eta}_y \end{pmatrix} \begin{pmatrix} u \\ v \end{pmatrix}. \tag{2}$$

And horizontal shear stress tensor is also

$$\begin{pmatrix} \tilde{\tau}_{\xi\xi} & \tilde{\tau}_{\xi\eta} \\ \tilde{\tau}_{\xi\eta} & \tilde{\tau}_{\eta\eta} \end{pmatrix} = \begin{pmatrix} \tilde{\xi}_x & \tilde{\xi}_y \\ \tilde{\eta}_x & \tilde{\eta}_y \end{pmatrix} \cdot \begin{pmatrix} \tau_{xx} & \tau_{xy} \\ \tau_{xy} & \tau_{yy} \end{pmatrix} \cdot \begin{pmatrix} \tilde{\xi}_x & \tilde{\xi}_y \\ \tilde{\eta}_x & \tilde{\eta}_y \end{pmatrix}^T. \tag{3}$$

Subscripts for the stress tensor indicate the surface and direction of the action.

Finally, basic equations on the unsteady 2D flow are obtained as following equations (4), (5) and (7).

$$\begin{aligned} &\frac{\partial \tilde{U}}{\partial t} h + \tilde{U} h \left\{ \frac{\partial \tilde{U}}{\partial \tilde{\xi}} - \tilde{J}(\tilde{V} - \tilde{U}\cos\theta^{\eta\xi}) \frac{\partial \theta^\xi}{\partial \tilde{\xi}} \right\} \\ &+ \tilde{V} h \left\{ \frac{\partial \tilde{U}}{\partial \tilde{\eta}} - \tilde{J}(\tilde{V} - \tilde{U}\cos\theta^{\eta\xi}) \frac{\partial \theta^\xi}{\partial \tilde{\eta}} \right\} \\ &= -gh \left\{ \frac{\partial \zeta}{\partial \tilde{\xi}} + \cos\theta^{\eta\xi} \frac{\partial \zeta}{\partial \tilde{\eta}} \right\} - \tau_{z\xi} \\ &+ \frac{1}{J} \left[\frac{\partial}{\partial \xi} \left(\frac{Jh}{d\xi} \tilde{\tau}_{\xi\xi} \right) + \frac{\partial}{\partial \eta} \left(\frac{Jh}{d\eta} \tilde{\tau}_{\xi\eta} \right) \right] \\ &- \tilde{J} h \left(-\tilde{\tau}_{\xi\xi} \cos\theta^{\eta\xi} + \tilde{\tau}_{\xi\eta} \right) \frac{\partial \theta^\xi}{\partial \tilde{\xi}} \\ &- \tilde{J} h \left(-\tilde{\tau}_{\xi\eta} \cos\theta^{\eta\xi} + \tilde{\tau}_{\eta\eta} \right) \frac{\partial \theta^\xi}{\partial \tilde{\eta}} \end{aligned} \tag{4}$$

$$\frac{\partial \widetilde{V}}{\partial t}h + \widetilde{U}h\left\{\frac{\partial \widetilde{V}}{\partial \widetilde{\xi}} + \widetilde{J}(\widetilde{U} - \widetilde{V}\cos\theta^{\eta\xi})\frac{\partial \theta^{\eta}}{\partial \widetilde{\xi}}\right\}$$
$$+\widetilde{V}h\left\{\frac{\partial \widetilde{V}}{\partial \widetilde{\eta}} + \widetilde{J}(\widetilde{U} - \widetilde{V}\cos\theta^{\eta\xi})\frac{\partial \theta^{\eta}}{\partial \widetilde{\eta}}\right\}$$
$$= -gh\left\{\cos\theta^{\eta\xi}\frac{\partial \varsigma}{\partial \widetilde{\xi}} + \frac{\partial \varsigma}{\partial \widetilde{\eta}}\right\} - \tau_{z\eta}$$
$$+\frac{1}{J}\left[\frac{\partial}{\partial \xi}\left(\frac{Jh}{d\xi}\widetilde{\tau}_{\eta\xi}\right) + \frac{\partial}{\partial \eta}\left(\frac{Jh}{d\eta}\widetilde{\tau}_{\eta\eta}\right)\right]$$
$$-\widetilde{J}(-\widetilde{\tau}_{\xi\xi} + \widetilde{\tau}_{\xi\eta}\cos\theta^{\eta\xi})\frac{\partial \theta^{\eta}}{\partial \widetilde{\xi}}$$
$$-\widetilde{J}(-\widetilde{\tau}_{\xi\eta} + \widetilde{\tau}_{\eta\eta}\cos\theta^{\eta\xi})\frac{\partial \theta^{\eta}}{\partial \widetilde{\eta}} \qquad (5)$$

where g is gravity acceleration; ς is water level; θ^{ξ} and θ^{η} are relative angels of contra-variant axis from a base angle, and

$$\frac{\partial}{\partial \widetilde{\xi}} = \frac{\partial}{(d\xi)\partial\xi}, \quad \frac{\partial}{\partial \widetilde{\eta}} = \frac{\partial}{(d\eta)\partial\eta}.$$

Horizontal stress terms are expressed as

$$\widetilde{\tau}_{\xi\xi} = 2\varepsilon\left[\left(\frac{\partial \widetilde{U}}{\partial \widetilde{\xi}} + \cos\theta^{\eta\xi}\frac{\partial \widetilde{U}}{\partial \widetilde{\eta}}\right)\right.$$
$$\left.-\widetilde{J}(-\widetilde{U}\cos\theta^{\eta\xi} + \widetilde{V})\left(\frac{\partial \theta^{\xi}}{\partial \widetilde{\xi}} + \cos\theta^{\eta\xi}\frac{\partial \theta^{\xi}}{\partial \widetilde{\eta}}\right)\right]$$
$$\widetilde{\tau}_{\xi\eta} = \varepsilon\left[\left(\cos\theta^{\eta\xi}\frac{\partial \widetilde{U}}{\partial \widetilde{\xi}} + \frac{\partial \widetilde{U}}{\partial \widetilde{\eta}}\right)\right.$$
$$\left.-\widetilde{J}(-\widetilde{U}\cos\theta^{\eta\xi} + \widetilde{V})\left(\cos\theta^{\eta\xi}\frac{\partial \theta^{\xi}}{\partial \widetilde{\xi}} + \frac{\partial \theta^{\xi}}{\partial \widetilde{\eta}}\right)\right]$$
$$+\varepsilon\left[\left(\frac{\partial \widetilde{V}}{\partial \widetilde{\xi}} + \cos\theta^{\eta\xi}\frac{\partial \widetilde{V}}{\partial \widetilde{\eta}}\right)\right.$$
$$\left.-\widetilde{J}(-\widetilde{U} + \widetilde{V}\cos\theta^{\eta\xi})\left(\frac{\partial \theta^{\eta}}{\partial \widetilde{\xi}} + \cos\theta^{\eta\xi}\frac{\partial \theta^{\eta}}{\partial \widetilde{\eta}}\right)\right]$$
$$\widetilde{\tau}_{\eta\eta} = 2\varepsilon\left[\left(\cos\theta^{\eta\xi}\frac{\partial \widetilde{V}}{\partial \widetilde{\xi}} + \frac{\partial \widetilde{V}}{\partial \widetilde{\eta}}\right)\right.$$
$$\left.-\widetilde{J}(-\widetilde{U} + \widetilde{V}\cos\theta^{\eta\xi})\left(\cos\theta^{\eta\xi}\frac{\partial \theta^{\eta}}{\partial \widetilde{\xi}} + \frac{\partial \theta^{\eta}}{\partial \widetilde{\eta}}\right)\right]$$

The bottom shear stresses $\tau_{\xi z}$ and $\tau_{\eta z}$ are evaluated from Manning's formula by using the absolute velocity;

$$\sqrt{u^2 + v^2} = \widetilde{J}\sqrt{\widetilde{U}^2 - 2\widetilde{U}\widetilde{V}\cos\theta^{\xi\eta} + \widetilde{V}^2},$$

physical contra-variant velocity vectors, water depth h and Manning's roughness coefficient n.

Horizontal eddy viscosity ε is expressed by the sum of $(\kappa u_* h)/6$ and eddy viscosity of Smagorinsky model in horizontal plane.

The local and convective acceleration terms in basic equations are rewritten as

$$\frac{\partial \widetilde{U}}{\partial t}h + \widetilde{U}h\frac{\partial \widetilde{U}}{\partial \widetilde{\xi}} + \widetilde{V}h\frac{\partial \widetilde{U}}{\partial \widetilde{\eta}}$$
$$= \left[\frac{\partial \widetilde{U}h}{\partial t} + \frac{d\xi}{J}\frac{\partial}{\partial \widetilde{\xi}}\left(\frac{J}{d\xi}\widetilde{U}\widetilde{U}h\right) + \frac{d\eta}{J}\frac{\partial}{\partial \widetilde{\eta}}\left(\frac{J}{d\eta}\widetilde{U}\widetilde{V}h\right)\right]$$
$$-\widetilde{U}\left[\frac{\partial h}{\partial t} + \frac{1}{J}\left\{\frac{\partial}{\partial \xi}\left(\frac{J\widetilde{U}h}{d\xi}\right) + \frac{\partial}{\partial \eta}\left(\frac{J\widetilde{V}h}{d\eta}\right)\right\}\right] \qquad (6)$$

Here, continuity equation is expressed as

$$J\frac{\partial h}{\partial t} + \frac{\partial}{\partial \xi}\left(\frac{J\widetilde{U}h}{d\xi}\right) + \frac{\partial}{\partial \eta}\left(\frac{J\widetilde{V}h}{d\eta}\right) = 0 \qquad (7)$$

As the equation (7) is satisfied, the equation (6) is calculated by using only the first terms in right hand side with a central finite differential method in conservation form. To the contrary, the 1st order upwind numerical viscous terms against left side of equation (6), i.e.

$$|\widetilde{U}|\,h\frac{d\xi}{2}\frac{\partial^2 \widetilde{U}}{\partial \widetilde{\xi}^2} + |\widetilde{V}|\,h\frac{d\eta}{2}\frac{\partial^2 \widetilde{U}}{\partial \widetilde{\eta}^2}$$

is added for avoiding the effect of water depth and metrics to the upwind scheme.

$(J/d\xi, J/d\eta)$ appearing in a conservative form of equations means covariant length of computational mesh in Figure 1 and its physical covariant length is directly used in the conservative form.

If contra-variant length and covariant length of computational mesh and angles of contra-variant axis are given, these equations can be solved with easiness in the orthogonal curvilinear coordinate system and accuracy in the general coordinate system. When the general coordinate system is orthogonal,

$$\cos\theta^{\eta\xi} = 0, \quad \widetilde{J} = 1.$$

When the coordinate system is oblique, the curvature terms become zero.

2.3 *Treatment of inundation front over the flood plain in the rising stage and abrupt bank step in the falling stage*

In an unsteady compound channel flow, the inundation of water over flood plain and falling of water from flood plain into main channel occur. If water depth

at flooding front is so small, computation cannot be performed well.

In this model, if water depth is less than 0.1 cm, its mesh is assumed "Dry" and the computation of flow at this front is performed by using only the local acceleration term, gravity force term and bottom shear stress term as shown in Figure 2.The velocity at the bank steps in falling stage is calculated by expressing water-surface slope term, bottom shear stress term and convective terms by only values of the flood plain in the following two cases as shown in Figure 3;

(1) When the water level in the main channel is below than the flood plain height.
(2) When the water level in the main channel is below than the flood plain water level and water depth over the flood plain is very small.

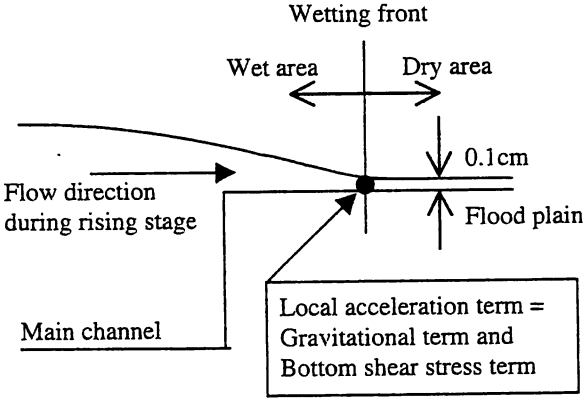

Figure 2. Treatment of inundation front over the flood plain and assumption for computation at inundation front.

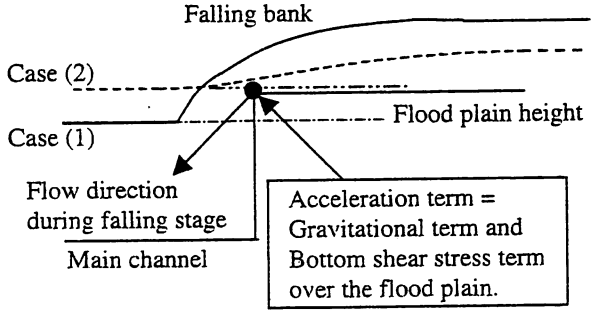

Figure 3. Treatment of falling water and assumption for computation at the falling bank.

In condition (1), the momentum from the flood plain by the convection except eddy viscous stress is transported to the main channel and water surface slope is discontinued at the bank step.

3 UNSTEADY FLOW ANALYSIS

3.1 *Hydraulic and computational conditions*

The computations of unsteady 2D flow are performed on a model channel and the Maruyama River observation reach as shown in Figures 4 and 5, respectively.

As shown in Figure 4, channel width is 2.2 m, main channel width is 0.5 m, main channel bank height is 0.045 m, sinuosity of meandering main channel is 1.02, bed slope is 1/1,000 and artificial grass is attached over the flood plain as roughness. In the computation for the model channel, the discharge hydrograph is given at the upstream end as shown in Figure 5, and the weir height at downstream end is kept constant. Values of Manning's roughness coefficient are 0.011 in the main channel and 0.024 at the flood plain. Number of computational grid points is 181 × 39. Computational time increment is Dt = 0.01 s.

The observation reach (15–10 km) of the Maruyama River is shown in Figure 3, where the discharge at the upstream end is not measured, but measured at the middle section of the reach. Figure 12 shows measured water surface profiles between the upstream and the downstream ends. In this analysis, water levels at upstream pond U and downstream pond D in Figure 5 were set virtually. Water levels at the ponds were adjusted so that the water levels computed at upstream and downstream ends of the observation reach might coincide with the observed hydro-graphs, instead of the discharge hydrograph at the upstream end. The cross-sectional shapes at upstream end (Section A), middle point (Section B) and downstream end (Section C) are shown in Figure 6. Main channel depth in the Maruyama River is about 3–4 m. There is a sand bar at the downstream end. At the initial state of the computation, the water level at No. A and No. C are 5.6 m and 2.6 m. The roughness of Maruyama River is unknown. Three combinations of roughness at the main channel and the flood plain were examined as shown in Table 1.

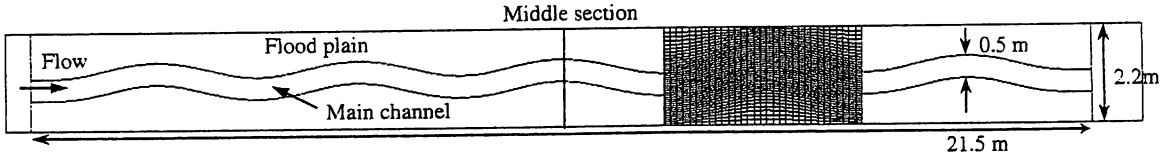

Figure 4. Layout of a model channel.

Figure 7 demonstrates discharge hydrographs at section B in three cases of Table 1. Although values of discharge change due to the difference of roughness, minimum change in shapes of hydrograph and times of the peak discharge are shown. Water surface profiles are shown in Figure 8. The three lines of the water surface profiles are almost same, even if the roughness and discharge change to a certain degree. Therefore, the peak discharge and velocity depend on the roughness of the river reach, but other hydraulic quantities may not change by these hydraulic parameters.

The discharge hydrograph in this computation depends on water level hydrograph at the upstream and downstream ends. As discharge in this computation depends on the accuracy of measured temporal change in water levels at the observation reach, field surveying is important for an analysis.

In this investigation, data set No. 2 in Table 1 is adopted as the values of Manning's roughness

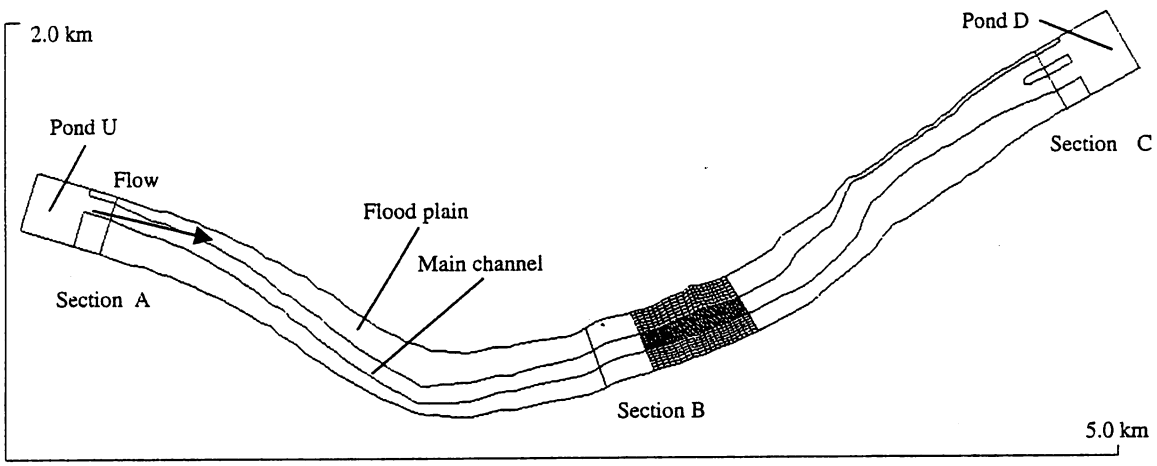

Figure 5. Observation reach of the Maruyama River.

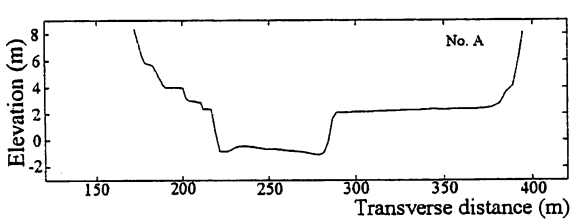

(a) Cross-sectional shape at section A

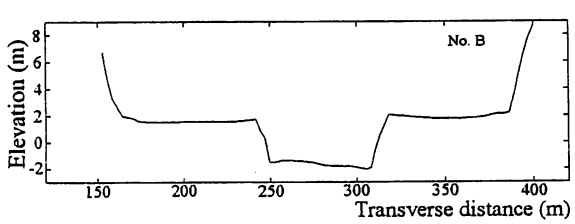

(b) Cross-sectional shape at section B

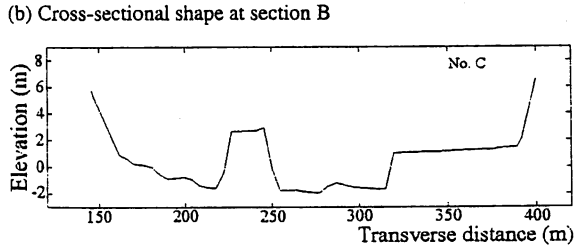

(c) Cross-sectional shape at section C

Figure 6. Cross-sectional shape in the observation reach of the Maruyama River.

Table 1. Relationship between the Manning's roughness coefficients and the peak discharge at the river reach.

Data set No.	Roughness in the main channel	Roughness over the flood plain	Peak discharge at the river reach (m^3/s)
1	0.030	0.040	2560–2650
2	0.030	0.038	2650–2700
3	0.025	0.035	2930–2970

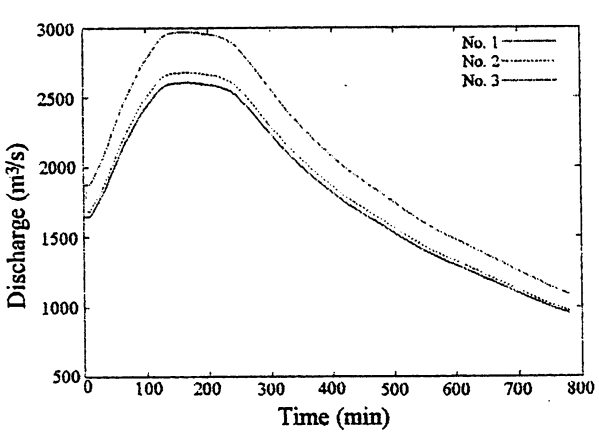

Figure 7. Temporal changes in discharge at section No. B.

coefficient to fit the computed discharge to the observed one, i.e. 2600–2700 m^3/s.

Number of computational grid points in all area is 231 × 29. Computational time increment Dt = 0.1 s.

3.2 *Computational results for flood flow of the model channel*

The hydrograph computed at the upstream and downstream ends in a compound meandering channel is shown in Figure 9. The discharge hydrograph is distorted in the downstream direction and the peak discharge is attenuated. This reduction of the peak discharge is due to the temporal and spatial change in water surface slope, storage of water in the channel and the momentum exchange between water in the main channel and the flood plain.

In the rising stage around 500 s, the downstream discharge decreases compared to the upstream because of the flooding over the flood plain and the storage of water in the channel. By the contrary, in the falling stage, the discharge at the downstream end increases around 1,500 s due to the release of the storage water.

The relationship between discharge at the upstream end and the depth at the middle section of the model channel is displayed in Figure 10. A path line representing this relationship draws a clockwise loop and the discharge at the rising stage is higher than one at the falling stage. The difference of discharge at the same water depth is maximum when depth = 5 cm, where the momentum is transported one-sidedly from a main channel to flood plain during rising stage or from flood plain to a main channel at the falling stage with a small relative depth. This difference becomes smaller due to the large momentum exchange between the main channel and the flood plain, as the relative depth becomes larger. The small difference at the large relative depth is mainly due to the change in the water surface slope.

Figure 11 shows the two relationships between velocity and water depth at the middle section of the channel. One is a result when the water level at downstream end is high. The other line is a result when water level at the downstream end is lower than the flood plain height. When the water level at downstream end is low, temporal increase of velocity is shown around

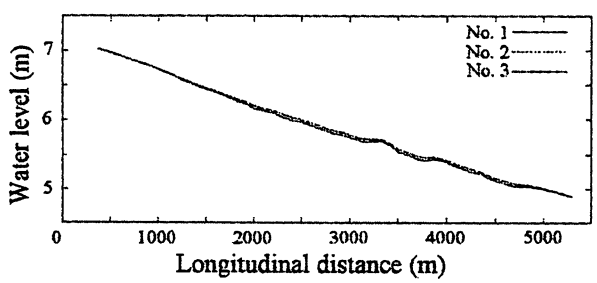

Figure 8. Longitudinal water surface profiles along the main channel at 180 min.

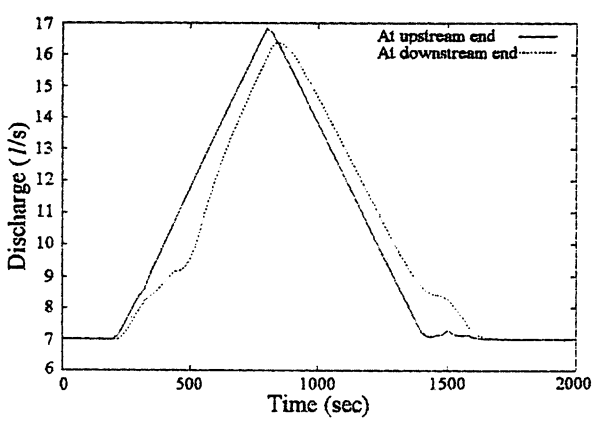

Figure 9. Temporal change in discharge at the upstream and downstream ends of the observation reach in a model channel.

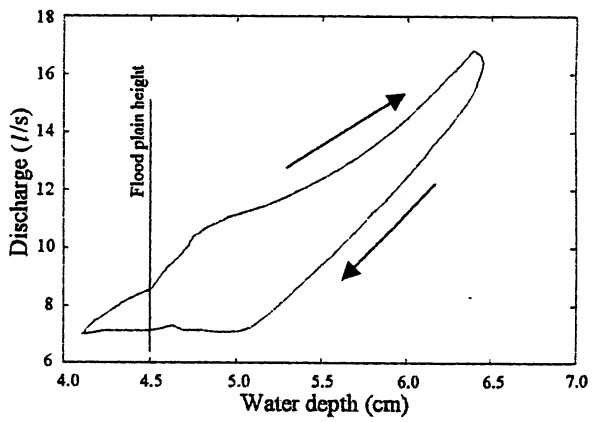

Figure 10. Relationship between the discharge and the water depth at the middle section of a model channel.

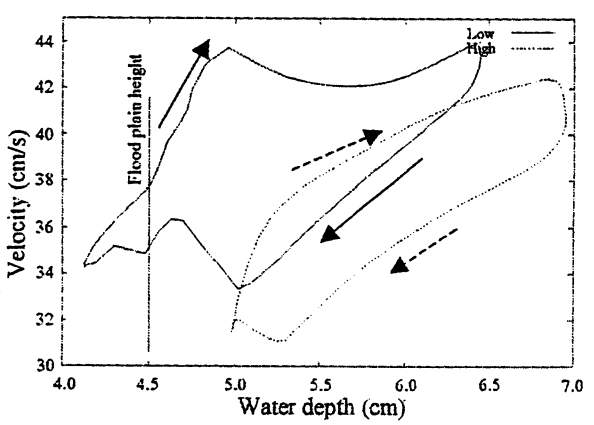

Figure 11. Relationship between the velocity and the water depth at the middle section of a model channel.

water depth = 5 cm in the rising stage. By the contrary, when water level at the downstream end is high, these hydraulic phenomena cannot be seen and this line forms a simple loop.

Therefore, it is considered that temporal increase in velocity in the main channel at the rising stage and temporal decrease of velocity at the falling stage are a characteristic phenomenon when the water level at downstream side is low. Because higher velocity flow goes from the main channel to the flood plain, the lower velocity flow on the flood plain cannot enter into the main channel in the rising stage.

In this case, there is no large additional resistance due to the momentum exchange between the main channel and the flood channel. Therefore, the velocity in the main channel increases temporally at the rising stage, until the momentum exchange become large. In the falling stage, because the lower velocity over the flood plain enters into the main channel, velocity in the main channel becomes low.

When the relative depth is large, the velocity in the main channel of compound meandering river is not so high because of the momentum exchange and roughness of flood plain. However, the computed velocity in the main channel at large relative depth is a little larger than the one measured in the model experiment. This difference of velocity at the large relative depth may be due to the character of the one layer model which cannot describe the three dimensional structure of flow in a compound meandering channel.

3.3 *Computation results of flood of the Maruyama River*

The computed and observed water levels at sections A, B and C are shown in Figure 12. The computed discharge at the sections A, B and C is presented in Figure 13. The computed water levels at upstream and downstream ends coincide with observed those above mentioned. As the initial condition is steady state, the temporal change in water level at section B is delayed little and the discharge at section C around 20 min decreases due to temporal reduction of water surface slope at the downstream end.

The discharge hydrograph changes in the downstream direction. The position of the peak discharge is shifted from left to right as flood progresses. The about 3% decrement of peak discharge is seen in the observation reach of the Maruyama River as shown in Figure 13. The peak discharge is reduced because of the storage water in the river reach. This change of peak discharge is due to the change in the water surface slope. As the difference between water levels at sections A and C becomes milder as time progress (Figure 12), the peak discharge decreases with time. Figure 14 demonstrates temporal change in mean water surface slope between upstream and downstream ends. Water slope decreases with time. After the peak of discharge, it becomes almost constant and its value is about 1/3000.

The relationships; water level versus discharge and water level versus velocity at section B are shown in Figures 15 and 16, respectively. As the water level at the downstream side was higher than the flood plain height and relative depth was large, flooding and falling at the step bank did not occur in the observation period on the Maruyama River.

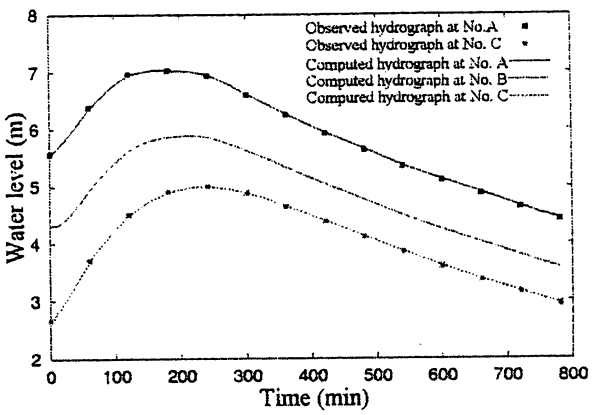

Figure 12. The temporal change in computed and observed water levels at section No. A, No. B and No. C.

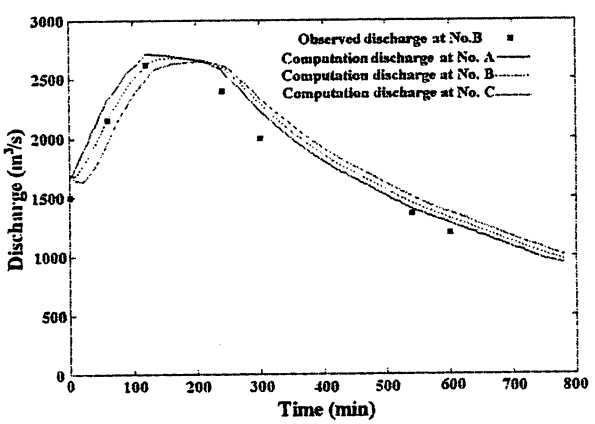

Figure 13. Temporal change in computed discharge at section No. A, No. B and No. C.

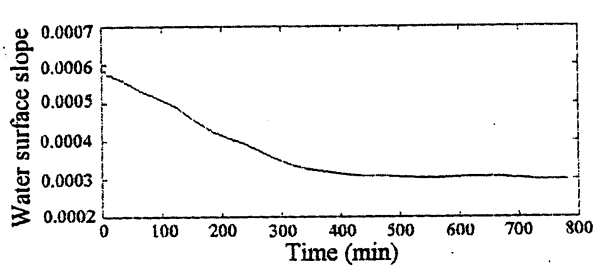

Figure 14. Temporal change in water surface slope between at upstream and downstream ends.

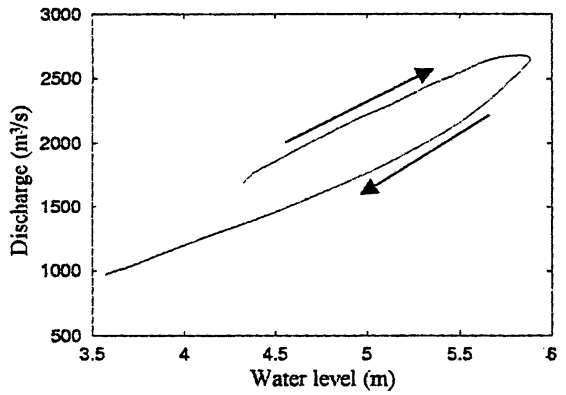

Figure 15. Relationship between water level and discharge at section No. B.

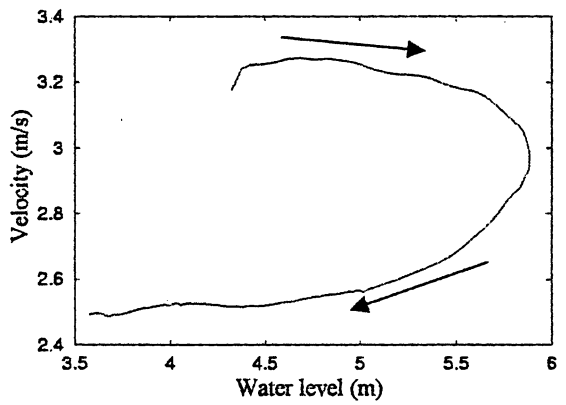

Figure 16. Relationship between water level and velocity at section No. B.

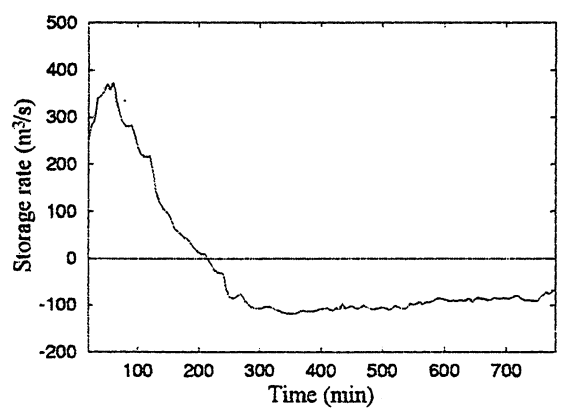

Figure 17. Temporal change in the storage rate at the Maruyama River reach.

So, both path lines on the discharge and the velocity draw the clockwise loops simply. The discharge and the velocity at rising stage are larger than those at falling stage, because the water surface slope at rising stage is larger than that at falling stage.

The temporal change of storage rate in this river reach is shown in Figure 17. The storage rate; i.e. the discharge difference between cross-section A and C, is about 100–300 m^3/s within a 5 km reach at the beginning of flooding. The peak of storage rate occurs before the peak of discharge. After the peak of discharge, the storage water in this reach is released at an almost constant value. Its rate is about 100 m^3/s.

4 CONCLUSION

The following conclusions were obtained for the downstream propagation and the distortion process of flood waves from laboratory experiments, field measurements and numerical computation.

(1) An unsteady two dimensional numerical model expressed by physical components of general curvilinear coordinate system was developed for a computational meandering channel flow. This model is applied for flood flows in the model channel and the Maruyama River, Japan. It was proved that the numerical model could evaluate the attenuation of the peak discharge and storage volume of flood flows and would be useful for any boundary conditions.

(2) During rising stage with the small relative depth, the momentum of main channel is transported toward the flood plain. At this moment flow from the flood plain toward the main channel hardly occur, therefore main channel flow is not influenced by the roughness of flood plain and velocity in the main channel increases with increasing depth. When momentum exchange between main channel and flood plain becomes large, the velocity in the main channel decreases temporally. When depth on the flood plain becomes large, the velocity in the main channel increases again because of high velocity on the flood plain.

(3) The reduction of peak discharge is calculated on flood in the Maruyama River. About 3% reduction of the peak discharge occurs for a flood wave propagation in about 5 km reach.

REFERENCES

Fukuoka, S., Watanabe, A., Seki, K. & Okabe, H., 2000. Effects of unsteadiness, plan form and cross-sectional form of channels on hydraulic characteristics of flood flow, Annual Journal of Hydraulic Engineering, JSCE, Vol. 44, pp. 867–872. (in Japanese)

Fukuoka, S., Seki, K., & Kuris, D., 2000. Flood flow storage and peak discharge attenuation in channels, Advances in Rive Engineering, Vol. 6, pp. 31–36 (in Japanese).

Fukuoka, S., 2000. Flow and topographic change in compound meandering rivers, Keynote lectures, 4th

International Conference on Hydro-Science and Engineering, CDROM.

Mutasingwa, A. G., Fukuoka, S. & Watanabe, A., 2001. Comparison between experiment and computed flood flow characteristics in a compound meandering channel, Annual Journal of Hydraulic Engineering, JSCE, Vol. 45, pp. 589–594.

Fukuoka, S. & Watanabe, A., 1998. Three dimensional analysis on flows in meandering compound channels, Journal of Hydraulic, Coastal and Environmental Engineering, JSCE, No. 586/II-42, pp. 39–50 (in Japanese)

Fukuoka, S. & Watanabe, A., 1999. Analysis of Bed Topography in a Compound Meandering Channel Using 3D Numerical with Assumption of Hydraulic Pressure, Journal of Hydro-science and Hydraulic Engineering, pp. 97–105.